The amorphous form of salsalate: experimental qualifications and predictability *in silico*

Matthew Habgood, Robert W. Lancaster, Milen Gateshki and Alan M. Kenwright

Amorphous solids challenge our understanding of phase behaviour. For small organic molecules, particularly pharmaceuticals, they also offer improved solubility and bioavailability. A computational approach to understanding of amorphous stability and ease of formation for such molecules would be valuable. An apparently ideal test case is salicylsalicylic acid (salsalate), which has been reported to form an amorphous phase that is long-term stable below and above its glass temperature. In this study we report the application of computational crystal structure prediction (CSP) techniques to salsalate, supported by an experimental investigation of the amorphous phase by solid form screening and X-ray derived pair distribution functions (PDFs). CSP reveals a pair of hydrogen bonding motifs that appear to be severely detrimental to the molecule's ability to pack efficiently and stably, indicating an explanation for salsalate's formation of a stable amorphous phase. However, experimental data cautions against overstating this stability. The amorphous phase is found to crystallize more readily, in a wider variety of conditions, and the molecule is more prone to thermal degradation than has been previously reported, giving rise to impurities that may frustrate crystallization.

1. Introduction

Though their theoretical description is an ongoing challenge,[1,2] the amorphous phases of small organic molecules are of great interest to the pharmaceutical industry. Newly-developed molecules frequently suffer problems[3] with bioavailability that threaten their usefulness *in vivo*. Amorphous phases, higher in energy and lower in structure, offer better bioavailability than their crystalline counterparts.[4-7] The primary concern is their propensity to transform into the more stable crystalline forms. Attention has therefore been directed to understanding the thermodynamic and kinetic factors affecting crystallization,[8,9] including the properties of the individual molecular species. Molecular properties that encourage amorphous formation have been suggested as high molecular weight with a high degree of branching or complexity, and hence high conformational variability;[9-11] absence of benzene rings;[10] a molecular shape that discourages or precludes close packing and hence crystallization;[12,13] and presence of electronegative atoms.[10] The last factor may be closely tied to the influence of hydrogen bonds; it has been observed that hydrogen bonding behaviour other than that found in the crystalline form seems to play a role in stabilizing amorphous phases[11,14,15] and indeed this concept has been used to design glass-forming molecules.[16] However it is clear that most of these are not fully reliable indicators of amorphous stability. There is no obvious boundary at which a molecule is sufficiently conformationally variable to have problems crystallizing. It is very difficult to tell whether an isolated molecule will pack well or badly. A molecule may be able to form hydrogen bonding motifs other than that found in a known crystal structure, but it is unlikely to be obvious whether these will stabilize an amorphous phase or promote alternative crystal structures. Benzene rings have formed an integral part of molecules specifically (and successfully) designed to be amorphous.[13]

An encouraging candidate for an *in silico* procedure to gain a clearer picture of a molecule's thermodynamic or kinetic resistance to crystallization from an amorphous solid may be crystal structure prediction (CSP).[17] Over the last few years, CSP has emerged as a powerful and increasingly accurate tool for computationally analysing the organic solid state. Software and algorithms now in use have proven capable of predicting the most stable crystal structure (polymorph) for small organic molecules,[18,19] and latterly large molecules typically associated with pharmaceutical APIs,[20] including in systems such as hydrates,[21] cocrystals,[22,23] and salts.[24,25] However, identifying one optimally stable crystal structure is only a part of the capabilities of CSP. Successful contemporary methods also produce a 'crystal energy landscape',[26] a set of hypothetical thermodynamically stable crystal structures. This landscape can be used to anticipate alternative, metastable polymorphs.[27-29] More generally, though, it can be used to gain an overview of the viable solid state interactions for a molecule. It is this application that has potential for helping to anticipate amorphous stability. By definition, crystal structures are not amorphous, but a suitably broad set of hypothetical crystal structures could show whether a molecule can only produce loosely packed, unstable crystal structures, or whether it has a possible hydrogen bonding motif that impedes the formation of a stable crystal structure. A crystal energy landscape was able to highlight such an equivalent family of motifs for the disordered structure of eniluracil.[30] It is therefore relevant to directly investigate whether a crystal energy landscape can help to predict the formation of a stable amorphous phase for a molecule.

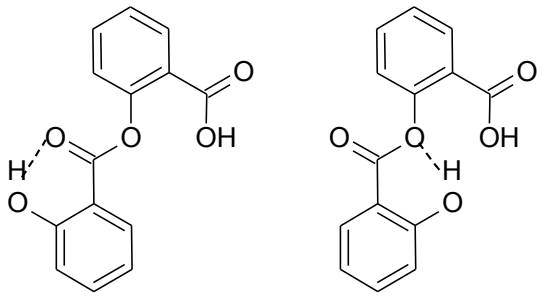

(a) (b)

Figure 1. Salsalate in the internally hydrogen bonded conformations found in the crystal structures; (a) major conformation and (b) minor conformation.

A good target molecule for such an investigation is salsalate (Fig.1), a non-steriodal anit-inflammatory drug (NSAID).[31] Salsalate has one crystal structure[32,33] reported in the Cambridge Structural Database (CSD[34]) (refcode WOQDAH[*]), which is disordered between two conformers in which the alcohol group forms an internal hydrogen bond to either the ester carbonyl oxygen (Figure 1(a)) or the ester ether oxygen (Figure 1(b)), with a ratio of ≈ 0.7:0.3. The modelling of this disorder using the method of symmetry-adapted ensembles[35,36] is considered in the supporting information, Section S1. Attention in this study will focus on the more stable major component; it is not believed that this will substantially alter the conclusions. Various melting points for crystalline salsalate are reported at ≈ 131 – 150°C. The formation

[*] On close inspection, the structures WOQDAH and WOQDAH01 turn out to be near-identical, with $RMSD_{15}$ = 0.054. Effectively, they are redeterminations of the same structure with a slightly different disorder model. For simplicity, the Z' = 1 determination WOQDAH01 is used in this study.

of a nematic phase at elevated temperatures close to the melting point has also been reported.[37] Most interestingly, despite being a relatively small molecule, it has been reported to readily form a viscous supercooled liquid phase that is long-term stable even at temperatures well above a glass transition at $T_g \approx 6°C$.[32,38,39] Indeed, it has been reported to be difficult to crystallize.[32] This exceptional behaviour invites study, as the molecule is not obviously consistent with any of the criteria noted above for stable amorphous phases.

This study represents an attempt to resolve this quandary, and assess the usefulness of crystal energy landscapes for amorphous phases, by generating and analysing a landscape for salsalate. Further experimental investigation has also been carried out to clarify aspects of the formation and structure of salsalate's amorphous phase. These include a limited solid form screen, infrared spectroscopy analysis of the amorphous and crystalline forms, NMR analysis of salsalate after formation of the amorphous phase by melting, and an attempt to determine any short-range structure in the amorphous form through X-ray derived pair distribution functions (PDFs) carried out by PANalytical B.V.

Finally, for comparison with the crystal energy landscape, an attempt was made to generate a computational model amorphous phase for salsalate. The best method for generating a simulation cell for such a model is not well-established. The classic method of cooling a simulated liquid ('bake-and-quench') is effective in some cases but leads to errors in others.[40] Successful results have been obtained in recent years[41-43] for large organic molecules using Monte Carlo-based cell construction routines developed for polymers.[44] In this study two approaches are compared: a bake and quench simulation, and a new approach based on 'melting' a computationally generated crystal structure by artificially ('alchemically') reducing the dispersion potential used in the model, with the objective of obtaining a model disordered phase that maintains the (electrostatically mediated) hydrogen bonding suggested by CSP.

2. Methods

2.1 Lattice energy model

The suitability of the selected lattice energy model was checked by geometrically minimizing the most common (major, Figure 1(a)) conformation of the molecule in the experimental crystal structure WOQDAH01.

Minimization was carried out using the program CrystalOptimizer,[45] which simultaneously relaxes the crystal structure and the internal degrees of freedom of the molecule. Lattice energies are calculated as $E_{latt} = U_{inter} + \Delta E_{intra}$, the intermolecular energy plus the change in the internal energy of the molecule relative to the gas phase conformation. Internal energies were calculated using parabolic local approximate models (LAMs) based on *ab initio* calculations on the isolated molecule at the HF/6-31G(d,p) level of theory. Intermolecular energies were calculated as the sum of a interactions between atom-centred distributed electrostatic multipoles, representing electrostatic interactions, and an atom-atom exponential-6 term representing all other interactions, particularly dispersion. Distributed multipoles were calculated from Stone's distributed multipole analysis (DMA) using the program[46,47] GDMA2.2,

based on analysis of a wavefunction calculated at the PBE0/6-31G(d,p) level of theory. Multipole interactions are handled by DMACRYS,[48] called internally by CrystalOptimizer. The exp-6 potential was taken from a set of parameters fitted to crystallographic and thermodynamic data, sometimes called the 'FIT potential'.[49-51]

All *ab initio* calculations were carried out using Gaussian03.[52]

Following minimization, the crystal structure was compared to the original experimental structure by calculating the root-mean-square difference of atomic positions on fifteen nearest-neighbour molecules ($RMSD_{15}$) using[53] Mercury3.0. Molecules are required to overlap to within distance tolerances of 20% and angle tolerances of 20° to be included in this measure. $RMSD_{15}$ was 0.20 Å with a density of 1.39 g cm^{-3}, a close match to the experimental[32] density of 1.40 g cm^{-3} at 293K. The lattice energy model therefore appears to be accurate.

2.2 Experimental Methods

Salicylsalicylic acid (98% purity) was obtained from Alfa Aesar and used without further purification. The manufacturers' stated melting point is 132 - 138°C, but was measured here as 131 - 145°C, and as stated in section 1 has been reported in other studies in the range 131 - 150°C.

Amorphous material was generated from the melt and a limited polymorph screen was carried out using the commercial material. Hot stage microscopy work was carried out using a Kofler stage (Reichert, Austria). Infrared spectra were obtained using a Perkin Elmer Spectrum One FTIR fitted with a diamond ATR accessory. Spectra were collected over the range 4000-650cm^{-1} at a resolution of 4cm^{-1}. X-ray powder diffraction measurements were made with samples presented in a sealed capillary. Pair distribution analysis was performed by Panalytical on a Empyrean diffraction system equipped with a programmable divergence slit and a X'Celerator detector (Mo Kα radiation used over the range 2-150° 2θ) with the sample again being prepared in a sealed capillary. Solution state NMR measurements were made using a Varian VNMRS-700 with samples dissolved in CDCl3 and referenced to tetramethylsilane.

2.3 Crystal Structure Prediction

Infrared spectroscopy indicated that the amorphous phase consisted entirely of conformers containing no internal hydrogen bond. The program CrystalPredictor[54] was therefore used to generate 400,000 structures of varying, non-internally hydrogen bonded conformations in 59 common space groups (including *Fdd*2, the experimental space group) using an approximate model of lattice energy replacing multipoles with point charges. The most stable generated structures were relaxed, and their energies refined, using CrystalOptimizer and the lattice energy model described in Section 2.1.

It was considered desirable to compare the lattice energies of these structures with that of the experimental crystal structure. It has been noted that the combination of intermolecular electrostatics calculated using distributed multipoles combined with internal energies calculated *ab initio* tends to overestimate the stability of internal relative to intermolecular hydrogen bonds,[55] making such comparisons difficult. The polarizable continuum model (PCM)[56] has been shown to approximately resolve this

difficulty. Recalculating multipoles and internal energies in a continuum that approximates a surrounding crystal structure polarizes the molecule and balances the energies of internal and intermolecular hydrogen bonds.[57] The energies of the crystal structures in this landscape and of the experimental structure were hence recalculated after CrystalOptimizer relaxation using the PCM, with $\varepsilon = 3$, a value typical of organic crystals.

2.4 A model amorphous phase

To generate a model of the amorphous phase of this potentially highly flexible molecule, the molecular dynamics package DL_POLY was selected.[58] Rather than rigorous accuracy, an approximate model for qualitative comparison with the crystal energy landscape was sought. Hence, electrostatics were represented using point charges derived using the CHelpG scheme[59] from the PCM wavefunction of the molecular conformation found in the 2nd ranked structure of the crystal energy landscape. All other internal and intermolecular terms were represented using the Dreiding potential.[60] Coefficients of the r^{-6} intermolecular (dispersion) term were adjusted to reproduce the experimental density (1.40 g cm^{-3}) in a simulation of a supercell of the experimental structure. The adjusted coefficients are given in Supporting Information, Section S2.

Two model amorphous phases were generated. The first, amorph_1, was generated using a 'bake-and-quench' method. A supercell of a randomly selected structure from the crystal energy landscape was heated up to 500K and hence melted. This was then cooled down in steps of 50K, each step run for 50ps, until it was returned to 298K. The second, amorph_2, was derived from the second ranked structure in the crystal energy landscape (see section 3.2), which contained a pseudo-polymeric one dimensional hydrogen bonding motif. A supercell of this structure was 'melted' by reducing the coefficient of the r^{-6} intermolecular (dispersion) term to 0.4 of its original value for a run of 100ps, then switching it back on in steps of 0.1 of the original value, each running for 50ps. The purpose was to generate an amorphous phase shaped by the strong hydrogen bonding motif generated in this crystal structure.

Both model amorphous phases were equilibrated for 200 ps, and then enthalpy, density, and hydrogen bonding connections were collected over a run of 1ns with a 1 fs timestep, at 298K and 1.01 bar. The NσT (constant composition, stress, and temperature) ensemble was maintained by the Nose-Hoover thermostat and barostat[61] with respective relaxation times of 0.1ps and 0.3ps.

3. Results

3.1 Experimental results

3.1.1 Solid form screening

A limited polymorph screen, on a small scale, was carried out in triplicate using 9 solvents. Apparently amorphous material was obtained from ethanol, acetonitrile (once), dioxane (once), and trifluoroethanol (once). The material showed no birefringence under polarised light microscopy and the internal hydrogen bonded OH observed in the IR spectrum of the known crystalline form had clearly been broken.

Crystalline material, with IR spectra corresponding to the commercial material was obtained from methanol, chloroform, acetonitrile (twice), hexane, acetone, dioxane (twice) and water.

An amorphous phase can be produced readily both from the melt and from the correct choice of solvent (particularly ethanol), and does indeed appear to be long term stable. It should be noted, though, that all attempts to reproduce the formation of the amorphous phase from solution on a scale larger than a few milligrams produced crystalline material. In addition, preparation by melting turned out to yield a variable but significant level of decomposition impurities unless the sample was prepared under nitrogen. See section 3.1.3.

3.1.2 Infrared spectroscopy

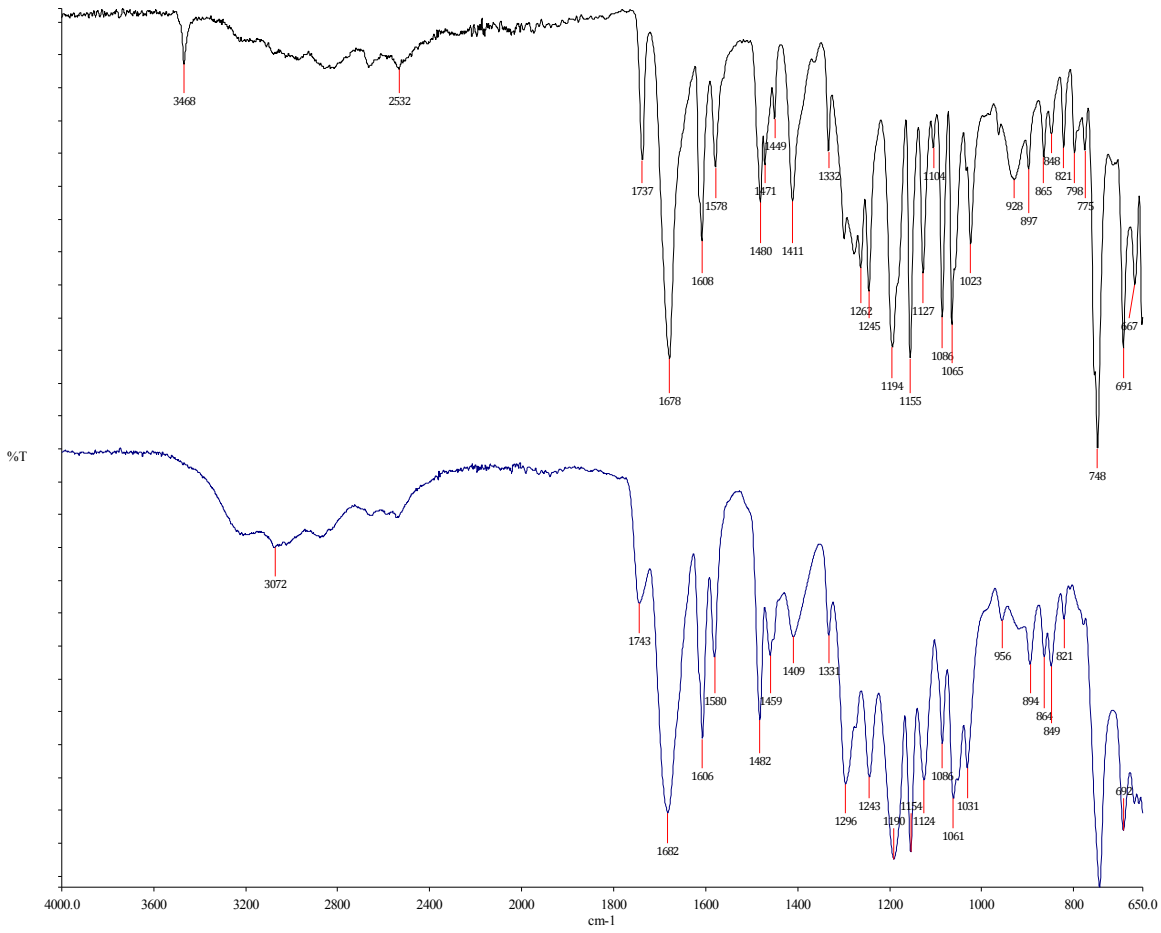

Figure 2. Infrared spectra for the crystalline (upper) and the amorphous (lower) forms of salsalate.

As can be seen in Figure 2, the band present at 3467 cm^{-1} in the crystalline spectrum, which is highly characteristic of salicylic internal hydrogen bonds,[62] is not present in the amorphous spectrum. This indicates that the amorphous phase contains predominantly conformations lacking the internal hydrogen bond.

3.1.3 Solution NMR

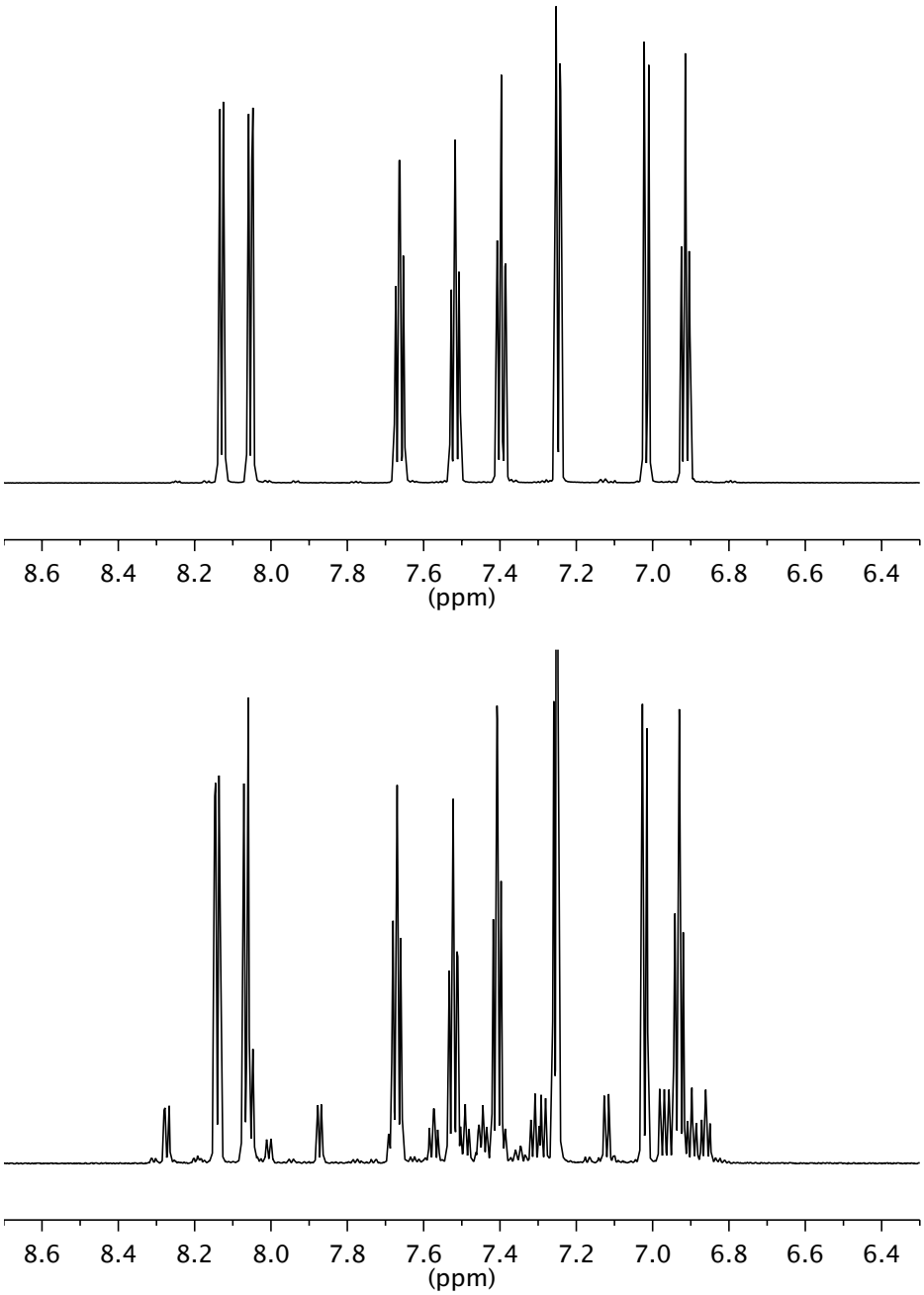

Figure 3. NMR spectra of salsalate (^{1}H, 700 MHz, $CDCl_3$). Upper: as purchased. Lower: after melting and re-solidifying (rapid cooling in liquid nitrogen).

Figure 3 shows the typical effect of trying to prepare samples of the amorphous form from the melt. The upper plot shows the aromatic region of the proton spectrum of salsalate as purchased. The lower plot shows the corresponding spectrum of a sample prepared by heating the "as purchased" material in a small open vial until it had just melted and then rapidly cooling the melted material using liquid nitrogen. Additional peaks, presumed to correspond to decomposition products, are evident, typically at around the 10 mole% level. Holding the sample at or around the melting point for longer results in rapid conversion to a wider range of products with the starting

material being present as only a fairly minor component after 30 minutes in the melt. Rapid heating and cooling of small amounts of the "as received" material in a capillary tube under nitrogen can produce small samples of amorphous material with substantially lower levels of impurities, but the levels of impurities present depend critically on the details of the preparation so obtaining truly reproducible samples of amorphous material from the melt is problematic.

3.1.4 X-ray PDFs

Plot here.

Figure 4. X-ray diffraction plots and PDFs for crystalline and amorphous salsalate.

X-ray diffraction plots (Figure 4) confirmed that a sample amorphous phase produced here is indeed X-ray amorphous. The PDF plots in Figure 4 indicate that the amorphous phase has no structure beyond a range of about ≈ 7 Å, and that within that range, what structure exists is very similar to the crystalline form. This could indicate that there is no intermolecular ordering at all in the amorphous phase, and that the whole PDF comes from the molecule itself. Alternatively, some hydrogen bonding motifs might give peaks at < 7 Å.

3.2 Crystal energy landscape

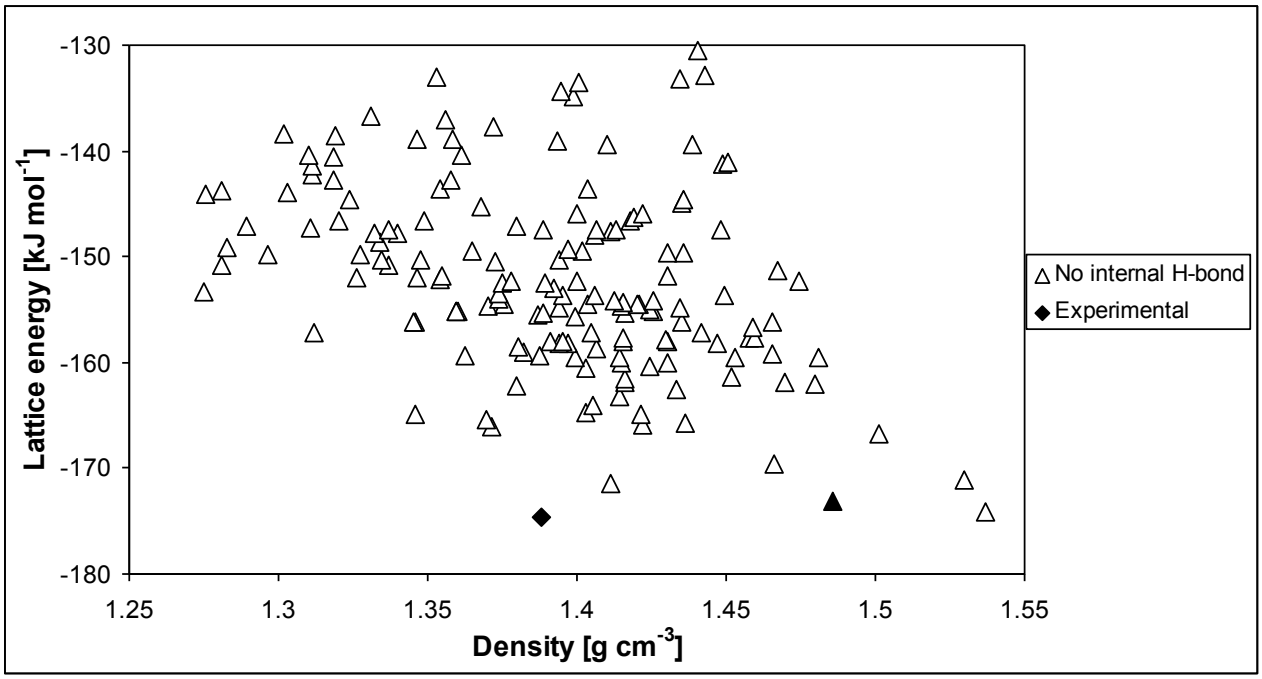

Figure 5. Crystal energy landscape for the non-internally hydrogen bonded conformations of salsalate. Each point is a crystal structure The (internally hydrogen bonded) experimental structure is also marked.

Figure 5 shows that the experimental structure is more stable than any of the hypothetical non-internally hydrogen bonded crystal structures, consistent with this being the only known crystal structure.

The second-ranked structure, marked with a filled triangle, is based a round a pseudo-polymeric one dimensional hydrogen bonding motif. This was used as the basis for a model amorphous phase, as noted in Section 2.4.

3.3 Model amorphous phases

Structure	ΔH_{sub} [kJ mol^{-1}]	Density [g cm^{-3}]
Experimental	-140.5	1.40
2nd ranked	-135.9	1.49
amorph_1	-120.2	1.35
amorph_2	-120.5	1.33

Table 2. Sublimation enthalpies and densities calculated by molecular dynamics using the Dreiding potential. Values for a supercell of the second ranked hypothetical structure, from which amorph_2 was derived, are included for comparison. ΔH_{sub} was calculated as $-U + RT - E_{mol}$, for total potential energy U, and average potential for a single isolated (gas phase) molecule of E_{mol}.

Table 2 shows that the sublimation enthalpies and densities calculated using the very approximate Dreiding-plus-charges potential used here are broadly consistent with the lattice energies and densities calculated using the more accurate potentials reported in Section 3.2 (the energy gap between the experimental and the 2nd ranked generated structure is 1.6 kJ mol^{-1} under that potential). The two amorphous structures are very similar in stability, and reasonably close to the experimentally reported[32] density of 1.35 g cm^{-3}, with amorph_1 having the closest match.

H-bond donation	% donors in amorph_1	% donors in amorph_2
Carboxyl group donation		
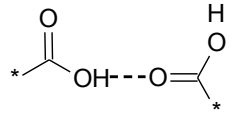	28	35
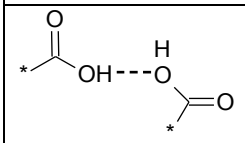	7	4
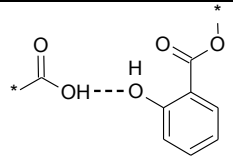	16	24
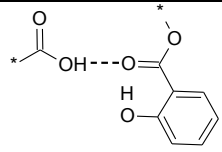	15	15

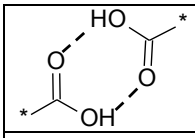	10	20
Alcohol group donation		
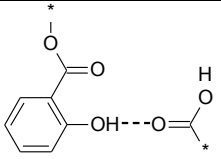	19	26
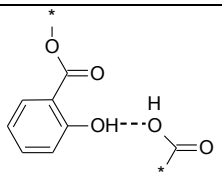	3	4
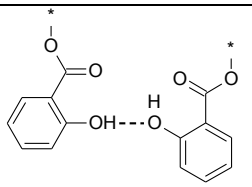	40	29
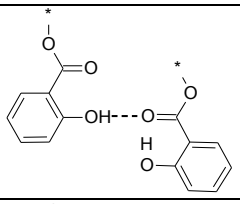	22	21
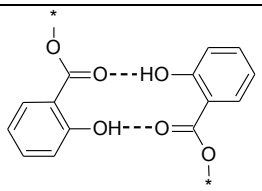	< 1	< 1

Table 3. Percentages of carboxyl and of alcohol hydrogens involved in different H-bonding motifs, on average, in the two model amorphous phases. A bond was defined as a hydrogen atom within 2.35 Å of the indicated acceptor atom.

The hydrogen bond motif frequencies in Table 3 must be interpreted with care, since the approximate, point charge-based model of electrostatics used for these calculations is known to be only partially adequate for the geometries and energies of hydrogen bonds, compared to distributed multipoles.[63,64] Given that the latter are not available for these calculations, the figures in Table 3 represent a working approximation.

More generally, radial distribution functions (not shown) calculated for both model amorphous cells are consistent with the experimental pair distribution functions (Section 3.1.4), in that there is no ordering beyond a distance of ≈ 7 Å.

4. Discussion

The experimental work presented here significantly qualifies the implications of previous reports[32,38] on the ease of preparing the amorphous phase of salsalate. It shows that crystalline salsalate can be prepared from a variety of solvents and that,

furthermore, attempts to generate amorphous salsalate from solution fail on a larger scale. It is not clear whether this is due directly to scale-up problems or whether salsalate is prone to seeding as more work is done in one location. Either way, production of amorphous salsalate appears to be more error-prone than suggested in early studies[32] and cited in more recent work.[37,38]

More significantly, the NMR studies performed here on salsalate dissolved from an amorphous phase prepared by melting indicate that the molecule will thermally decompose, yielding a significant proportion of impurities in material prepared by this route. Identification of these impurities was not carried out in the context of this work, but a previous study[65] suggests that, dependent on conditions, salsalate will thermally decompose to varying proportions of salicylic acid, phenyl salicylate, and larger ester oligomers, either linear or cyclic. A significant proportion even of lower molecular weight impurities may disrupt any crystal structure formation and help produce an amorphous phase, but ester polymers, with their higher degree of conformational variability, are even more likely to do so. These results hence suggest that the ready formation and long lifetime of amorphous salsalate may not be due entirely to properties of the molecule itself, but to impurities that are readily formed during preparation of that phase. Nevertheless, it seems unlikely that these impurities can be entirely responsible for the phase behaviour, and hence it is still worth investigating what the favoured solid state interactions of the salsalate molecule, inferred from the crystal energy landscape, can imply about this issue.

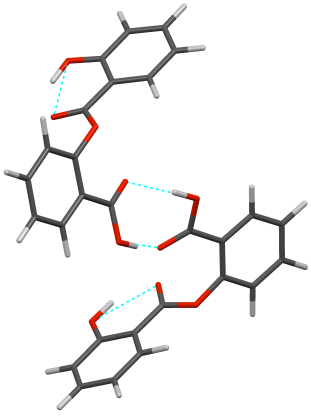

(a)

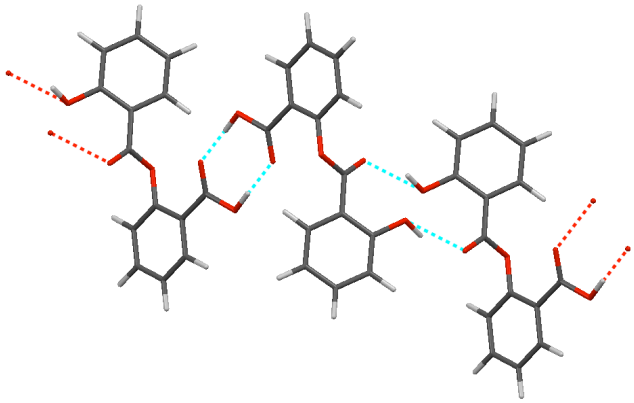

(b)

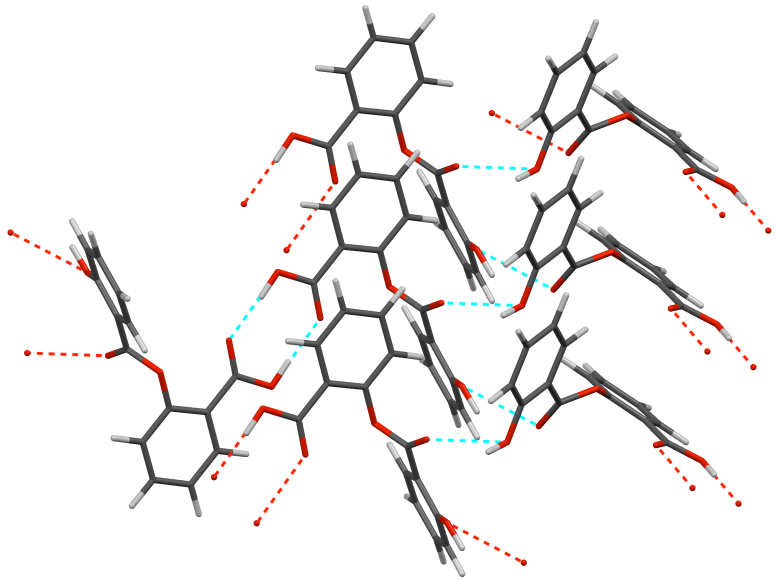

(c)

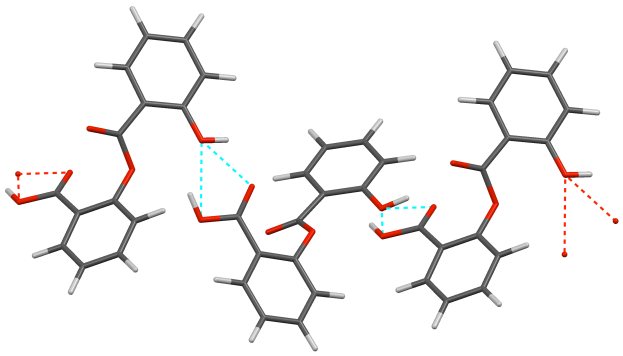

(d)

Figure 6. Hydrogen bonding motifs from the crystal energy landscape of salsalate: (a) reciprocal carboxylic acid bonding, in the (internally hydrogen bonded) experimental structures, (b) a 'pseudo-polymer' chain built via reciprocal carboxylic acid bonding and reciprocal alcohol – ester carbonyl bonding, (c) reciprocal carboxylic acid bonded dimers connected into a catemer by alcohol – ester carbonyl bonding, (d) a catemer based around carboxylic acid – alcohol bonding.

The crystal energy landscape for the non-internally hydrogen bonded conformers of salsalate (Figure 5) shows that the most stable of these structures is almost as stable as the experimental structure (the global minimum is 0.4 kJ mol^{-1} less stable), which is consistent with the formation of a solid phase from these conformers. Indeed, the stability of the amorphous phase with respect to the experimental crystal structure is explained by the differing conformers, as elucidated by the infrared spectrum (Figure 2). Rearrangement of the molecule's conformation and hence the entire hydrogen bonding network presents a considerable kinetic barrier. However, this does not explain why a crystal structure containing a non-internally hydrogen bonded conformation should not form. The landscape offers two different explanations for this phenomenon. The first of these comes from the second ranked structure. The hydrogen bonding in this structure (Figure 6 (b)) consists of one dimensional chains

of double-hydrogen-bonded molecules. Along with conformational variability of salsalate around the ester bonds, this suggests the possibility of 'pseudo-polymeric' behaviour, in which these kind of hydrogen bonded chains can adopt many different conformations, all of which would be similarly stable. The barrier to crystallization would then be essentially entropic: many different non-crystalline arrangements of these chains would be almost as stable as the crystal structure, hence crystallization would require a minimally guided search in a large conformation space.

Further examination of the crystal energy landscape, though, does not support this explanation. If it were true, a large number of crystal structures would be expected with the same hydrogen bonding motif packed in different ways (essentially, the projection of the supposedly large conformation space onto the space of periodic arrangements). This is not the case. Only a small number of other generated crystal structures contain the same motif. Further, an attempt was made to generate an amorphous crystal structure that contained the postulated pseudo-polymers (amorph_2, see Sections 2.4, 3.3). However, without the support of the close crystal packing, this hydrogen bonding motif collapsed, giving rise to a wide variety of differing motifs.

The second explanation offered for the failure of the non-internally hydrogen bonded conformations to crystallize comes from a pair of different hydrogen bonding motifs. The first of these consists of dimers built from reciprocally hydrogen bonded carboxylic acid groups, linked into catemers by bonds from the alcohol group to the ester carbonyl oxygen (Figure 6 (c)) ('catemers-of-dimers'). The second consists of catemers held together by carboxylic acid to alcohol hydrogen bonding (Figure 6 (d)) ('acid-alcohol catemers'). Structures containing these motifs share several qualities. They are relatively unstable: the most stable catemer-of-dimers structure is 9 kJ mol^{-1} above the global minimum, and the most stable acid-alcohol catemer structure is 8.5 kJ mol^{-1} above the global minimum. Moreover both of these structures are notably stabilized by electrostatic intermolecular forces (which in this molecule will largely mean hydrogen bonding), with respectively 56% and 49% of their intermolecular potentials coming from electrostatics, as calculated by DMACRYS.[48] Both motifs also enforce relatively low density structures: the most dense catemer-of-dimers structure has 1.44 g cm^{-3}, while the densest acid-alcohol catemer structure has 1.48 g cm^{-3}, both of which are notably low compared to the global minimum structures density (also the highest density on the landscape) of 1.54 g cm^{-3}. Finally, both motifs are exceptionally well represented in the crystal energy landscape. Examining structures within 30 kJ mol^{-1} of the global minimum, ≈33% contain the catemer-of-dimers motif, and ≈25% contain the acid-alcohol catemer motif. Hence, overall, both motifs are associated with sets of crystal structures that cover a wide range of packings, but which tend to be relatively poorly packed, as demonstrated by their relatively low density, relatively low stability compared to the global minimum, and reliance on electrostatic interactions, hence on the hydrogen bonding motifs itself, for cohesion.

In summary, the crystal energy landscape presents two hydrogen bonding motifs, either (or both) of which are good candidates to hinder crystallization, under the amorphous-forming mechanism proposed by (among others) Wang et al.[15] This explanation appears to be well supported by the landscape and is tentatively advanced

as the basis of salsalate's amorphous stability, possibly alongside contamination by thermal decomposition products.

Both model amorphous phase models support this explanation to an extent. Both have significant proportions of carboxyl to carboxyl and alcohol to ester hydrogen bond donation, consistent with the catemers-of-dimers motif; both also have significant proportions of carboxyl to alcohol and alcohol to carboxyl to alcohol donation, consistently with the acid-alcohol catemer motif. In this sense, both models can be said to support a combination of the two motifs as a basis for the amorphous phase. However, both also have significant proportions of alcohol-alcohol hydrogen bonding, a motif which only appears in a very few, unstable structures in the crystal energy landscape. The reasons for this difference are not clear, and may reflect the lower accuracy of the point-charge electrostatics model used in these simulations.

Unfortunately, even with experimental PDF data it is not possible to make a firm judgement as to which method of generating an amorphous phase was superior for salsalate, since the properties calculated here (stability, density, hydrogen bonding patterns) are very similar for both models. On the other hand, the similarity of the results between the two models adds confidence that no important information was missed in the direct modelling of amorphous phases.

Conclusions

Experimental work carried out in this study has shown that the reported stability and ready formation of salsalate's amorphous phase may be partly due to a significant proportion of impurities, some of them extended ester oligomers, that readily form by thermal decomposition, for example during melting. Nonetheless, properties of the molecule itself must be partly responsible for the observed robustly amorphous behaviour. A crystal energy landscape has suggested that this may be due to the formation of one or more hydrogen bonding motifs (a catemer made up of reciprocally bonded carboxylic acid pairs, and a carboxylic acid – alcohol catemer) that have difficulty in packing, resulting in low-density structures that are unstable relative to the global minimum and reliant on hydrogen bonding for cohesiveness. This explanation if consistent with previous observations of molecules that are able to form glasses stabilized by specific, badly crystallizing hydrogen bonding motifs. Molecular dynamics simulations of two model amorphous phases agreed with each other and broadly support this explanation, although the accuracy of the two models proved difficult to verify.

Although crystal structure prediction can obviously not be applied directly to amorphous phases, this study demonstrates that it can still be very useful in explaining, and perhaps eventually in qualitatively predicting, the formation and stability of amorphous phases.

Acknowledgements

Robin Harris, David Apperley, Paul Hodgkinson, Martin Vickers, James Patterson and Sally Price for useful discussions. PANalytical B.V. for instrument time. Ramsay Memorial Fellowship Trust for funding (MH).

Reference List

1. Debenedetti, P. G.; Stillinger, F. H. *Nature* **2001,** *410*, 259-267.
2. Berthier, L.; Biroli, G. *Reviews of Modern Physics* **2011,** *83*, 587-645.
3. Thayer, A. M. *Chemical & Engineering News* **2010,** *88*, 13-18.
4. Yu, L. *Adv.Drug Deliver.Rev.* **2001,** *48*, 27-42.
5. Murdande, S. B.; Pikal, M. J.; Shanker, R. M.; Bogner, R. H. *J.Pharm.Sci.* **2010,** *99*, 1254-1264.
6. Babu, N. J.; Nangia, A. *Crystal Growth and Design* **2011,** *11*, 2662-2679.
7. *Polymorphism in the Pharmaceutical Industry;* Wiley-VCH: Weinheim, 2006.
8. Bhugra, C.; Pikal, M. J. *J.Pharm.Sci.* **2008,** *97*, 1329-1349.
9. Baird, J. A.; van Eerdenbrugh, B.; Taylor, L. S. *J.Pharm.Sci.* **2010,** *99*, 3787-3806.
10. Mahlin, D.; Ponnambalam, S.; Hockerfelt, M. H.; Bergstrom, C. A. S. *Molecular Pharmaceutics* **2011,** *8*, 498-506.
11. Kim, S. J.; Karis, T. E. *J.Mater.Sci.* **1995,** *10*, 2128-2136.
12. Shirota, Y. *J.Mater.Chem.* **2000,** *10*, 1-25.
13. Mastrangelo, J. C.; Conger, B. M.; Chen, S. H. *Chem.Mater.* **1997,** *9*, 227-232.
14. Tang, X. C.; Pikal, M. J.; Taylor, L. S. *Pharmaceut.Res.* **2002,** *19*, 477-483.
15. Wang, R.; Pellerin, C.; Lebel, O. *J.Mater.Chem.* **2009,** *19*, 2747-2753.
16. Meunier, A.; Lebel, O. *Organic Letters* **2010,** *12*, 1896-1899.
17. Price, S. L. *Int.Rev.Phys.Chem.* **2008,** *27*, 541-568.
18. Day, G. M. et al. *Acta Crystallogr., Sect.B* **2009,** *65*, 107-125.
19. Bardwell, D. A. et al. *Acta Crystallogr., Sect.B* **2011,** *67*, 535-551.
20. Kazantsev, A. V.; Karamertzanis, P. G.; Adjiman, C. S.; Pantelides, C. C.; Price, S. L.; Galek, P. T.; Day, G. M.; Cruz-Cabeza, A. J. *Int.J.Pharm.* **2011,** *418*, 168-178.
21. Braun, D. E.; Karamertzanis, P. G.; Price, S. L. *Chem.Commun.* **2011,** *47*, 5443-5445.

22. Karamertzanis, P. G.; Kazantsev, A. V.; Issa, N.; Welch, G. W. A.; Adjiman, C. S.; Pantelides, C. C.; Price, S. L. *J.Chem.Theory Comput.* **2009,** *5*, 1432-1448.

23. Habgood, M.; Deij, M. A.; Mazurek, J.; Price, S. L.; ter Horst, J. H. *Cryst.Growth Des.* **2010,** *10*, 903-912.

24. Mohamed, S.; Tocher, D. A.; Price, S. L. *Int.J.Pharm.* **2011,** *418*, 187-198.

25. van de Streek, J.; Neumann, M. A.; Perrin, M. A. *CrystEngComm* **2010,** *12*, 3827-3833.

26. Price, S. L. *Accounts Chem.Res.* **2009,** *42*, 117-126.

27. Hamad, S.; Moon, C.; Catlow, C. R. A.; Hulme, A. T.; Price, S. L. *J.Phys.Chem.B* **2006,** *110*, 3323-3329.

28. Arlin, J. B.; Price, L. S.; Price, S. L.; Florence, A. J. *Chem.Commun.* **2011,** *47*, 7074-7076.

29. Habgood, M. *Phys.Chem.Chem.Phys.* **2012,** *14*, 9195-9203.

30. Copley, R. C. B.; Barnett, S. A.; Karamertzanis, P. G.; Harris, K. D. M.; Kariuki, B. M.; Xu, M. C.; Nickels, E. A.; Lancaster, R. W.; Price, S. L. *Cryst.Growth Des.* **2008,** *8*, 3474-3481.

31. Ross, M. B. *Hospital Formulary* **1991,** *26*, 803.

32. Greener, B.; Archibald, S. J.; Hodkinson, M. *Angew.Chem.,Int.Ed.* **2000,** *39*, 3601-3604.

33. Cox, P. J.; Gilmour, G. I.; MacManus, S. M. *Int.J.Pharm.* **2000,** *204*, 133-136.

34. Allen, F. H. *Acta Crystallogr., Sect.B* **2002,** *58*, 380-388.

35. Grau-Crespo, R.; Hamad, S.; Catlow, C. R. A.; de Leeuw, N. H. *Journal of Physics: Condensed Matter* **2007,** *19*, Art-256201.

36. Habgood, M.; Grau-Crespo, R.; Price, S. L. *Phys.Chem.Chem.Phys.* **2011,** *13*, 9590-9600.

37. Ramos, J. J. M.; Diogo, H. P.; Godinho, M. H.; Cruz, C.; Merkel, K. *J.Phys.Chem.B* **2004,** *108*, 7955-7962.

38. Digo, H. P.; Pinto, S. S.; Ramos, J. J. M. *J.Therm.Anal.Calorim.* **2004,** *77*, 893-904.

39. Graeser, K. Investigations of drug polyamorphism. University of Otago, 2009.

40. Biswas, P.; Tafen, D. N.; Inam, F.; Cai, B.; Drabold, D. A. *J.Phys,-Condens.Mat.* **2009,** *21*, 084207.

41. Simperler, A.; Kornherr, A.; Chopra, R.; Bonnet, P. A.; Jones, W.; Motherwell, W. D. S.; Zifferer, G. *J.Phys.Chem.B* **2006,** *110*, 19678-19684.

42. Gupta, J.; Nunes, C.; Vyas, S.; Jonnalagadda, S. *J.Phys.Chem.B* **2011,** *115*, 2014-2023.

43. Abdel-Halim, H.; Traini, D.; Hibbs, D.; Gaisford, S.; Young, P. *Eur.J.Pharm.Biopharm.* **2011,** *78*, 83-89.

44. Theodorou, D. N.; Suter, U. W. *Macromolecules* **1985,** *18*, 1467-1478.

45. Kazantsev, A. V.; Karamertzanis, P. G.; Adjiman, C. S.; Pantelides, C. C. *J.Chem.Theory Comput.* **2011,** *7*, 1998-2016.

46. Stone, A. J. *J.Chem.Theory Comput.* **2005,** *1*, 1128-1132.

47. *GDMA: A Program for Performing Distributed Multipole Analysis of Wave Functions Calculated Using the Gaussian Program System,* version 2.2; Stone, A. J. University of Cambridge: Cambridge, United Kingdom, 2010

48. Price, S. L.; Leslie, M.; Welch, G. W. A.; Habgood, M.; Price, L. S.; Karamertzanis, P. G.; Day, G. M. *Phys.Chem.Chem.Phys.* **2010,** *12*, 8478-8490.

49. Williams, D. E.; Starr, T. L. *Computers & Chemistry* **1977,** *1*, 173-177.

50. Cox, S. R.; Hsu, L. Y.; Williams, D. E. *Acta Crystallogr., Sect A.* **1981,** *37*, 293-301.

51. Coombes, D. S.; Price, S. L.; Willock, D. J.; Leslie, M. *J.Phys.Chem.* **1996,** *100*, 7352-7360.

52. *Gaussian 03,* Frisch, M. J. et al. Gaussian Inc.: Wallingford CT, 2004

53. Macrae, C. F.; Bruno, I. J.; Chisholm, J. A.; Edgington, P. R.; McCabe, P.; Pidcock, E.; Rodriguez-Monge, L.; Taylor, R.; van de Streek, J.; Wood, P. A. *J.Appl.Crystallogr.* **2008,** *41*, 466-470.

54. Karamertzanis, P. G.; Pantelides, C. C. *Mol.Phys.* **2007,** *105*, 273-291.

55. Karamertzanis, P. G.; Day, G. M.; Welch, G. W. A.; Kendrick, J.; Leusen, F. J. J.; Neumann, M. A.; Price, S. L. *J.Chem.Phys.* **2008,** *128*, 244708-244717.

56. Cossi, M.; Scalmani, G.; Rega, N.; Barone, V. *J.Chem.Phys.* **2002,** *117*, 43-45.

57. Cooper, T. G.; Hejczyk, K. E.; Jones, W.; Day, G. M. *J.Chem.Theory Comput.* **2008,** *4*, 1795-1805.

58. Smith, W.; Forester, T. R. *J.Mol.Graphics* **1996,** *14*, 136-141.

59. Breneman, C. M.; Wiberg, K. B. *J.Comput.Chem.* **1990,** *11*, 361-373.

60. Mayo, S. L.; Olafson, B. D.; Goddard, W. A. *J.Phys.Chem.* **1990,** *94*, 8897-8909.

61. Hoover, W. G. *Physical Review A* **1985,** *31*, 1695-1697.

62. Bellamy, L. J. *The infrared spectra of complex molecules;* Third ed.; 1975.

63. Buckingham, A. D.; Fowler, P. W. *Can.J.Chem.* **1985,** *63*, 2018-2025.

64. Price, S. L. *J.Chem.Soc.Faraday T.* **1996,** *92*, 2997-3008.

65. Shulga, O.; Dunn, J. *Thermochimica Acta* **2004,** *410*, 15-21.